REPORT

QUANTUM ELECTRONICS

Strongly correlated quantum walks with a 12-qubit superconducting processor

Zhiguang Yan[1,2]*, Yu-Ran Zhang[3,4,5]*, Ming Gong[1,2]*, Yulin Wu[1,2], Yarui Zheng[1,2], Shaowei Li[1,2], Can Wang[1,2], Futian Liang[1,2], Jin Lin[1,2], Yu Xu[1,2], Cheng Guo[1,2], Lihua Sun[1,2], Cheng-Zhi Peng[1,2], Keyu Xia[6,7,4], Hui Deng[1,2], Hao Rong[1,2], J. Q. You[8,3], Franco Nori[4,9], Heng Fan[5,10]†, Xiaobo Zhu[1,2]†, Jian-Wei Pan[1,2]

Quantum walks are the quantum analogs of classical random walks, which allow for the simulation of large-scale quantum many-body systems and the realization of universal quantum computation without time-dependent control. We experimentally demonstrate quantum walks of one and two strongly correlated microwave photons in a one-dimensional array of 12 superconducting qubits with short-range interactions. First, in one-photon quantum walks, we observed the propagation of the density and correlation of the quasiparticle excitation of the superconducting qubit and quantum entanglement between qubit pairs. Second, when implementing two-photon quantum walks by exciting two superconducting qubits, we observed the fermionization of strongly interacting photons from the measured time-dependent long-range anticorrelations, representing the antibunching of photons with attractive interactions. The demonstration of quantum walks on a quantum processor, using superconducting qubits as artificial atoms and tomographic readout, paves the way to quantum simulation of many-body phenomena and universal quantum computation.

Quantum walks (QWs) are the quantum mechanical analogs of classical random walks, describing the propagation of quantum walkers on a lattice (*1*, *2*). Different from classical random walks, QWs generate large-scale quantum superposed states and entanglement, allowing for classically unavailable applications, such as simulating many-body quantum biological, chemical, and physical systems (*3*), and for developing quantum algorithms exponentially faster than classical computation (*4*). QWs have been investigated in many physical systems, including photons (*5*, *6*), nuclear magnetic resonance (*7*), trapped ions (*8*, *9*), superconducting qubits (*10*), and neutral atoms (*11*, *12*). These studies are useful for further studies on quantum dynamical phenomena such as entangled state engineering (*13*), dynamical phase transition (*14*), and thermalization versus localization (*15*, *16*).

In systems with finite-range interactions, QWs of a single particle show the propagation of correlations within a linear light cone limited by the Lieb-Robinson bounds (*17*), implemented in a chain of seven ion spins for entanglement (*18*). Multiparticle QWs in interacting systems—for example, the Bose-Hubbard model (*19*)—are capable of performing universal quantum computation (*4*, *20*). Here we investigated the continuous-time QWs (*2*) of one and two strongly correlated microwave photons on a 12-qubit superconducting processor (Fig. 1) using superconducting qubits as artificial atoms with high-fidelity manipulation and tomographic readout. We observed fundamental quantum effects, including light cone–like propagation of quantum information of superposed states, in particular, entanglement between qubit pairs, and exotic behaviors of time-evolved correlations, representing photon antibunching with attractive interactions.

To preserve and observe the quantum features of QWs, a low-decoherence system capable of simultaneous readouts and high-precision full controls is required. In our experiment, QWs of photons are performed on a one-dimensional (1D) array of 12 coupled superconducting transmon qubits of the Xmon variety (Q_j, with j varied from 1 to 12), which has a decreased sensitivity to charge noise (*21*–*23*). This system can be described by the Bose-Hubbard model with the Hamiltonian (we set $\hbar = 1$, where $\hbar$ is Planck's constant h divided by 2π) (*15*, *19*, *22*)

$$H = J\sum_{j=1}^{11}\left(\hat{a}_j^{\dagger}\hat{a}_{j+1} + \text{h.c.}\right) + \frac{U}{2}\sum_{j=1}^{12}\hat{n}_j(\hat{n}_j - 1) + \sum_{j=1}^{12}h_j\hat{n}_j \qquad (1)$$

where $\hat{a}_j^{\dagger}$ ($\hat{a}_j$) is the bosonic creation (annihilation) operator, $\hat{n}_j = \hat{a}_j^{\dagger}\hat{a}_j$ is the number operator,

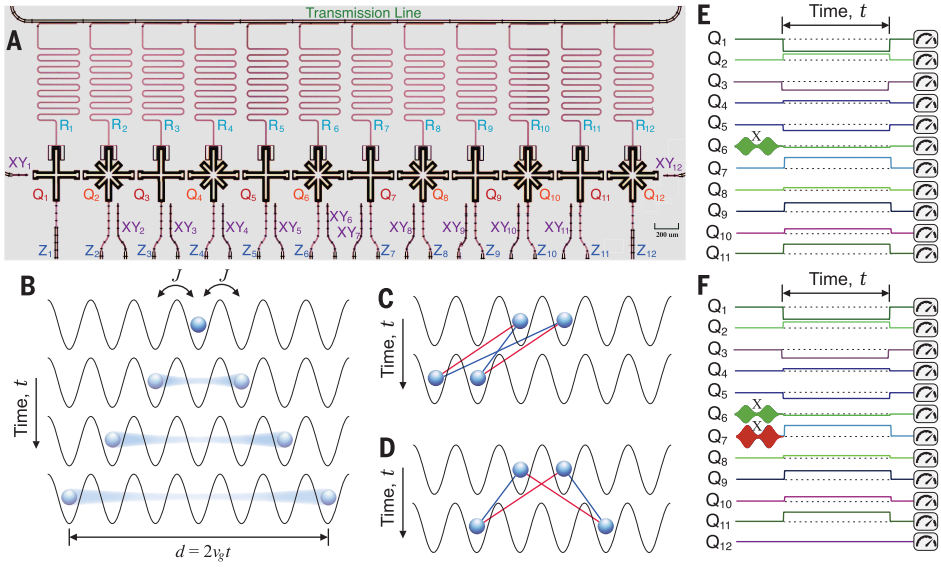

Fig. 1. QWs of one and two photons in a 1D lattice of a superconducting processor. (**A**) Optical micrograph of the 12-qubit chain sample. Each qubit has an independent microwave line for XY control and flux bias line for Z control, which is coupled to a separate $\lambda/4$ readout resonator (R) connected to the transmission line for measurements. (**B**) Starting from a localized initial state by exciting the central qubit (Q_6). The distance of the spread of nonlocal correlations is $d = 2v_g t$, with v_g being the group velocity of a walker. (**C**) For weakly interacting photons, QWs starting with initially localized two-photon states implement photon bunching (HBT effects). (**D**) For two strongly interacting photons, QWs display antibunching and fermionization of photons. (**E** and **F**) Experimental waveform sequences for single-photon QWs (E) and two-photon QWs (F). All qubits are initially prepared at $|0\rangle$ at their idle points, and then one or two qubits are transformed to $|1\rangle$ by an X gate. After the free evolution with a time t with all qubits tuned to the working point, all qubits are measured at their idle points.

Downloaded from https://www.science.org at Westlake University on May 17, 2024

J is the nearest-neighbor hopping strength, U is the on-site nonlinear interaction, h_j is the tunable on-site potential, and h.c. is the Hermitian conjugate. During the quench dynamics, all the on-site potentials are tuned to the same $h_j = h$. The experimental details of our system can be found in the supplementary materials.

For one-photon QWs, we used 11 superconducting qubits by turning Q_{12} off (see supplementary materials). With 11 superconducting qubits initialized at their idle points, we prepared the localized state using an X gate with Gaussian-enveloped microwave pulses (*24*) on the target superconducting qubit (Fig. 1E). Then, all qubits are biased to the working point (4.88 GHz) using the Z pulses, for the quench dynamics with a time t. After turning off the Z pulses to tune the qubits back to their idle points, the single-photon density distribution $p_j(t) = \langle \hat{n}_j \rangle$ can be read out simultaneously for all the qubits using a single transmission line coupled to each qubit's readout resonator (*25*). The density distributions of single-photon QWs are obtained by averaging 1000 repeated single-shot measurements for the initially centrally localized, leftmost-localized, and rightmost-localized states (Fig. 2, A to C, compared with the numerical simulations, Fig. 2, D to F, respectively). To study the high coherence generated in the QWs, we investigated the fidelity $F(t) = \sum_{j=1}^{11} \sqrt{p_j(t) q_j(t)}$ for the measured and theoretical probability distributions $p_j(t)$ and $q_j(t)$ (Fig. 3A). The high fidelity (greater than 90% within 100 ns) indicates that our experimental results are consistent with the theoretical predictions within the decoherence time (see also the comparisons in the supplementary materials). For the propagation of one photon starting from the central qubit, the single-qubit von Neumann entropy, $S = -\mathrm{Tr}(\rho \log \rho)$, where ρ is the density matrix, is measured by performing full tomography measurements on a single qubit (Fig. 3B), which reveals the spread of information and the nonlocal correlations with other qubits.

Furthermore, to observe the time evolution of nonlocal correlations, we implemented full tomography measurements on all reduced two-qubit states. We first consider the two-site correlation function $C_{ij}(t) = \langle \hat{\sigma}_i^z \hat{\sigma}_j^z \rangle - \langle \hat{\sigma}_i^z \rangle \langle \hat{\sigma}_j^z \rangle$ with $\hat{\sigma}_j^z \equiv |0\rangle_j\langle 0| - |1\rangle_j\langle 1|$ and plot the time evolution of the averaged correlation function $\bar{C}_d(t) \equiv (11-d)^{-1} \sum_{j=1}^{11-d} C_{j,j+d}(t)$ (Fig. 3D), where d is the distance between two qubits, which also reveals the light cone–like spread of correlations (*18*, *26*). Here, $\hat{\sigma}^\alpha$ with $\alpha = x, y, z$ are Pauli matrices on the $|0\rangle$ and $|1\rangle$ subspace. Figure 3E shows the entanglement propagation of two qubits located symmetrically around the central qubit. The entanglement measure of a mixed state ρ of two qubits used here is the concurrence (*27*)

$$E(\rho) = \max\{0, \lambda_1 - \lambda_2 - \lambda_3 - \lambda_4\} \quad (2)$$

where $\lambda_1, \ldots, \lambda_4$ are eigenvalues listed in decreasing order of the Hermitian matrix $R = (\rho^{\frac{1}{2}} \tilde{\rho} \rho^{\frac{1}{2}})^{\frac{1}{2}}$, with $\tilde{\rho} = (\hat{\sigma}^y \otimes \hat{\sigma}^y)\rho^*(\hat{\sigma}^y \otimes \hat{\sigma}^y)$ being the spin-flipped state of ρ. In contrast to classical random walks, the quantum dynamics with diffusive expansion of equal pairs of Gaussian-distribution waves, together with entanglement propagation, can be described by the coherent interference of quasiparticle modes of the collective behavior of the system (*18*).

Because longer-range interactions in our system can be neglected, compared with the nearest-neighbor ones, the propagation speed of quantum information is limited by the maximal group speed $v_g^{\max}$, known as the Lieb-Robinson bound (*17*). It exhibits a linear light cone with exponentially decaying tails analogous to the causal light cones arising in relativistic theories, which has been previously observed in different physical systems (*18*, *26*, *28*). For only nearest-neighbor interactions, the photon density propagation, after a local excitation at the j-th qubit, has a tighter bound $\langle \hat{n}_i \rangle \le I_d(4gt)$ (*29*), where $I_d(x)$ is the modified Bessel function of the first kind, $g = \max(J_{j,j+1})$, and $d = |i-j|$. In Fig. 3C, we compare the waves of density distributions of qubits from Q_7 to Q_{11} with the upper bounds $I_d(4gt)$ corresponding to shaded forbidden areas, showing that the nearest-neighbor cases can be well captured by the Lieb-Robinson bounds. The maximum propagation velocity, the linear fitting analyses of the group speeds of the concurrence,

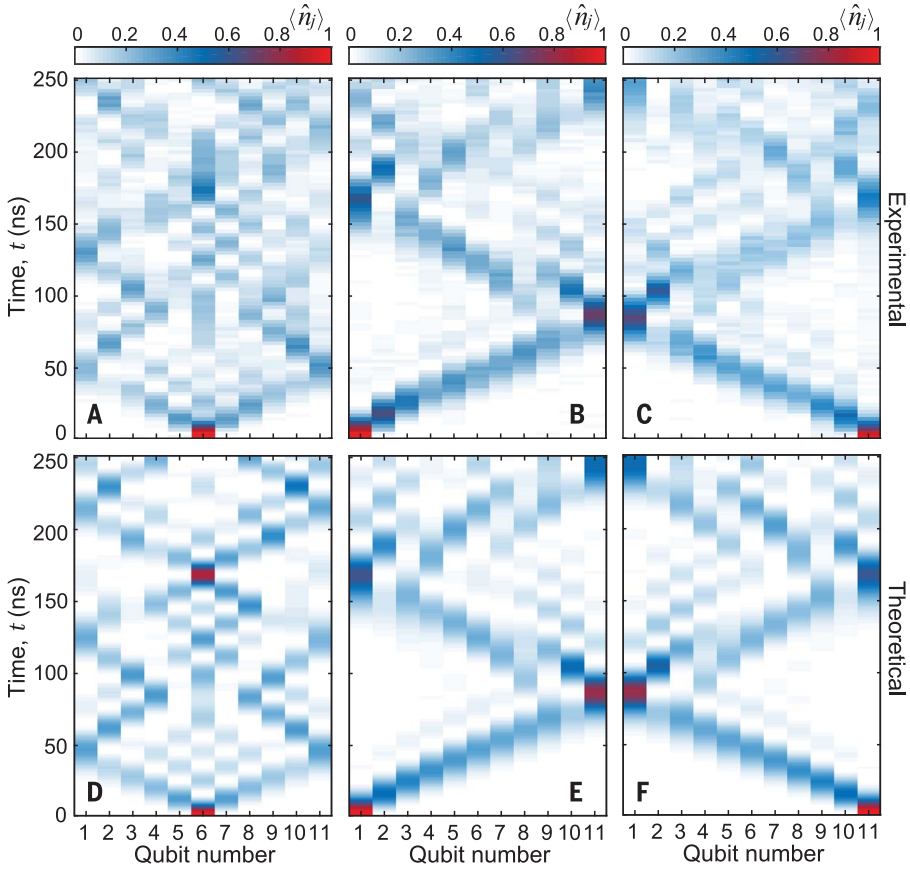

Fig. 2. QWs of a single photon in a 1D array of 11 superconducting qubits (from Q_1 to Q_{11}). (**A** to **F**) The time evolution of the density distribution $\langle \hat{n}_j \rangle$ of the quench after the initially localized state by placing one microwave photon into the central qubit Q_6 (A), the leftmost qubit Q_1 (B), and the rightmost qubit Q_{11} (C), compared with the numerical simulations (D), (E), and (F), respectively. Eleven superconducting qubits are used to allow a symmetric propagation in (A).

[1]Hefei National Laboratory for Physical Sciences at Microscale and Department of Modern Physics, University of Science and Technology of China, Hefei, Anhui 230026, China. [2]Shanghai Branch, CAS Center for Excellence and Synergetic Innovation Center in Quantum Information and Quantum Physics, University of Science and Technology of China, Shanghai 201315, China. [3]Beijing Computational Science Research Center, Beijing 100094, China. [4]Theoretical Quantum Physics Laboratory, RIKEN Cluster for Pioneering Research, Wako-shi, Saitama 351-0198, Japan. [5]Beijing National Laboratory for Condensed Matter Physics, Institute of Physics, Chinese Academy of Sciences, Beijing 100190, China. [6]National Laboratory of Solid State Microstructures, College of Engineering and Applied Sciences, and School of Physics, Nanjing University, Nanjing 210093, China. [7]Collaborative Innovation Center of Advanced Microstructures, Nanjing University, Nanjing 210093, China. [8]Department of Physics and State Key Laboratory of Modern Optical Instrumentation, Zhejiang University, Hangzhou, Zhejiang 310027, China. [9]Physics Department, University of Michigan, Ann Arbor, MI 48109-1040, USA. [10]CAS Center for Excellence in Topological Quantum Computation, University of Chinese Academy of Sciences, Beijing 100190, China.
*These authors contributed equally to this work.
†Corresponding author. Email: hfan@iphy.ac.cn (H.F.); xbzhu16@ustc.edu.cn (X.Z.)

Downloaded from https://www.science.org at Westlake University on May 17, 2024

von Neumann entropy, and density distributions are shown in the supplementary materials.

Finally, we demonstrate the QWs of two indistinguishable photons (*30*) with an array of 12 superconducting qubits in the presence of strong attractive interactions (*12*) (Fig. 1F). Strongly correlated multiparticle QWs are believed to have higher quantum complexity than the single-particle case and are capable of realizing universal quantum computation (*4*). In addition, two-photon QWs can demonstrate the Hanbury Brown-Twiss (HBT) interference (*6*), and the dynamical behaviors of the QWs are sensitive to the particle statistics. In the Bose-Hubbard model, for weakly interacting photons

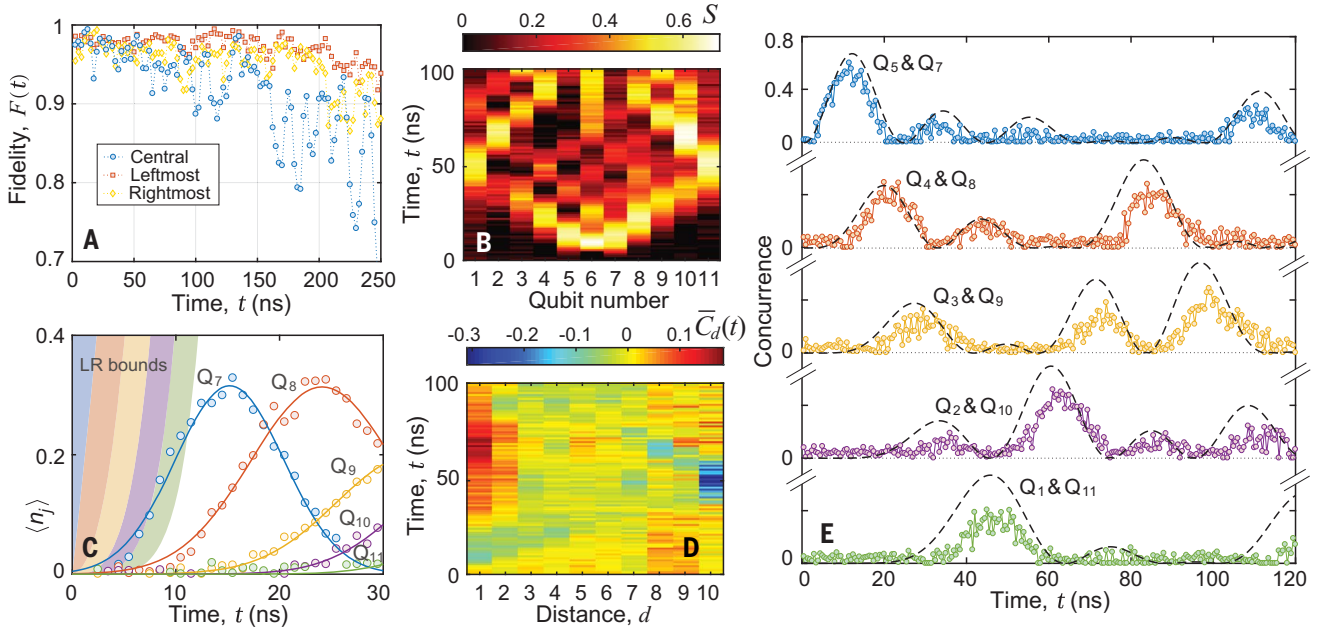

Fig. 3. Propagation of quantum information in the QWs of a single photon with a 1D array of 11 superconducting qubits (from Q_1 to Q_{11}). (**A**) The fidelity for the measured and theoretical probability distributions with respect to the centrally localized (blue circles), leftmost-localized (red squares), and rightmost-localized (yellow diamonds) initial states, respectively. (**B**) The time evolution of the single-qubit von Neumann entropy S. (**C**) Lieb-Robinson (LR) bounds [shaded forbidden areas with boundaries given by $l_d(4gt)$, color matched for different qubits] capture most of the signal of the density spreading (from Q_7 to Q_{11}). Solid curves are for the Gaussian fitting analyses of the wavefronts of the density. (**D**) The time evolution of the averaged two-qubit correlation function $\bar{C}_d(t)$ versus the distance d between two qubits. (**E**) Propagation of entanglement (concurrence) between pairs of qubits located symmetrically around the central qubit Q_6. The second and third wavefronts that are due to the quantum interference and reflection of the photon are clearly shown.

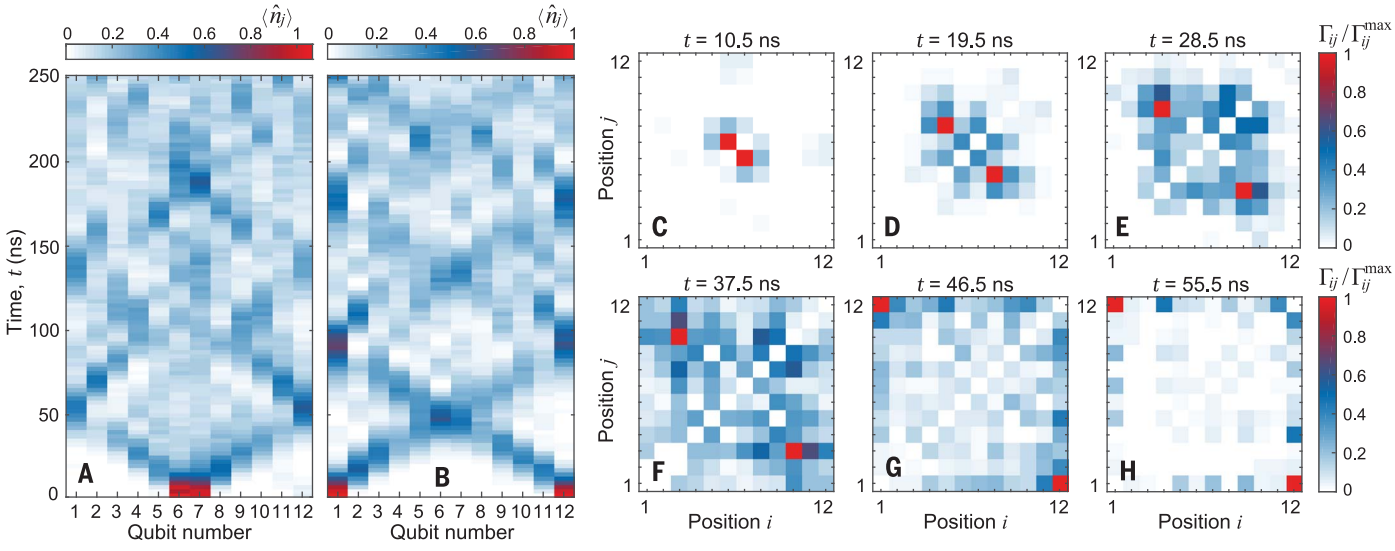

Fig. 4. Photon antibunching and fermionization in QWs with two identical photons on a 1D array of 12 superconducting qubits. (**A** and **B**) The time evolution of the density distribution $\langle \hat{n}_j \rangle$ after two photons placed into two adjacent central qubits (Q_6 and Q_7) (A) and two boundary qubits (Q_1 and Q_{12}) (B), respectively. (**C** to **H**) The normalized two-site correlators $\Gamma_{ij}/\Gamma_{ij}^{max}$ measured during the QWs of two strongly correlated photons at different evolution times. The long-range anticorrelations are clearly observed in the 1D Bose-Hubbard model with strong attractive on-site interactions, which reveal the photon antibunching and fermionization.

Downloaded from https://www.science.org at Westlake University on May 17, 2024

$|U| \ll J$, QWs starting from two adjacent excited qubits exhibit photon bunching (Fig. 1C), whereas for strongly interacting photons $|U| \gg J$, QWs of two adjacent photons display photon antibunching and fermionization (Fig. 1D). These different features of the HBT interference of boson- and fermion-like particle statistics can be distinguished by measuring the density-density correlators (*12*)

$$\Gamma_{ij} = \langle \hat{a}_i^\dagger \hat{a}_j^\dagger \hat{a}_i \hat{a}_j \rangle \quad (3)$$

where the measurements contributing to the diagonal elements of the correlator were neglected because of the low double-occupation probability (see supplementary materials).

In Fig. 4, A and B, we show the time evolution of the density distribution after two identical photons placed at two adjacent central qubits (Q_6 and Q_7) and two boundary qubits (Q_1 and Q_{12}), respectively. Both cases show higher quantum complexity of quasiparticle dynamics than the single-photon QWs. For the Bose-Hubbard Hamiltonian (Eq. 1), the behavior of the HBT interference, bosonic or fermionic, depends on the dimensionless ratio U/J (*30*). For $U/J \to 0$, it describes free bosons, whereas for $|U/J| \to \infty$, the model describes hard-core bosons. Because our 1D bosonic system has attractive (negative) interactions $-U/J \simeq 16$ or $20 \gg 1$, the emergence of photon antibunching, fermionization, and spatial anticorrelations are similar to those of noninteracting spinless fermions (*19*). However, the time evolutions of the density distributions are also similar to those of noninteracting bosons (see supplementary materials). In Fig. 4, C to H, we clearly observed anticorrelations compared with the free-boson cases, where composite probabilities concentrate around the diagonal of the normalized correlator $\Gamma_{ij}/\Gamma_{ij}^{\max}$, which demonstrates the process of fermionization of two interacting photons by repeating QWs. Because $U < 0$ in our system, we have also verified that the spatial anticorrelations by QWs with the two-particle HBT interference depend on the strength of the interaction but not on its sign (*30*).

We experimentally demonstrated QWs of one and two strongly interacting photons in a 1D array of superconducting qubits with short-range interactions. We observed the light cone–like propagation of quantum information, especially entanglement, and the photon antibunching with the two-photon HBT interference. Our results would be scalable to a few tens of qubits beyond classical simulation and lay the foundation for further studies on many-body dynamical phenomena and universal quantum computation.

REFERENCES AND NOTES

1. Y. Aharonov, L. Davidovich, N. Zagury, *Phys. Rev. A* **48**, 1687–1690 (1993).
2. E. Farhi, S. Gutmann, *Phys. Rev. A* **58**, 915–928 (1998).
3. I. Buluta, F. Nori, *Science* **326**, 108–111 (2009).
4. A. M. Childs, D. Gosset, Z. Webb, *Science* **339**, 791–794 (2013).
5. B. Do *et al.*, *J. Opt. Soc. Am. B* **22**, 499–504 (2005).
6. A. Peruzzo *et al.*, *Science* **329**, 1500–1503 (2010).
7. C. A. Ryan, M. Laforest, J. C. Boileau, R. Laflamme, *Phys. Rev. A* **72**, 062317 (2005).
8. H. Schmitz *et al.*, *Phys. Rev. Lett.* **103**, 090504 (2009).
9. P. Richerme *et al.*, *Nature* **511**, 198–201 (2014).
10. V. V. Ramasesh, E. Flurin, M. Rudner, I. Siddiqi, N. Y. Yao, *Phys. Rev. Lett.* **118**, 130501 (2017).
11. M. Karski *et al.*, *Science* **325**, 174–177 (2009).
12. P. M. Preiss *et al.*, *Science* **347**, 1229–1233 (2015).
13. M. Gong *et al.*, *Phys. Rev. Lett.* **122**, 110501 (2019).
14. J. Zhang *et al.*, *Nature* **551**, 601–604 (2017).
15. P. Roushan *et al.*, *Science* **358**, 1175–1179 (2017).
16. K. Xu *et al.*, *Phys. Rev. Lett.* **120**, 050507 (2018).
17. E. H. Lieb, D. W. Robinson, *Commun. Math. Phys.* **28**, 251–257 (1972).
18. P. Jurcevic *et al.*, *Nature* **511**, 202–205 (2014).
19. M. A. Cazalilla, R. Citro, T. Giamarchi, E. Orignac, M. Rigol, *Rev. Mod. Phys.* **83**, 1405–1466 (2011).
20. M. S. Underwood, D. L. Feder, *Phys. Rev. A* **85**, 052314 (2012).
21. J. Q. You, X. D. Hu, S. Ashhab, F. Nori, *Phys. Rev. B* **75**, 140515 (2007).
22. J. Koch *et al.*, *Phys. Rev. A* **76**, 042319 (2007).
23. R. Barends *et al.*, *Nature* **508**, 500–503 (2014).
24. E. Lucero *et al.*, *Phys. Rev. A* **82**, 042339 (2010).
25. K.-Q. Huang *et al.*, *Chin. Phys. B* **26**, 094203 (2017).
26. M. Cheneau *et al.*, *Nature* **481**, 484–487 (2012).
27. W. K. Wootters, *Phys. Rev. Lett.* **80**, 2245–2248 (1998).
28. T. Fukuhara *et al.*, *Nature* **502**, 76–79 (2013).
29. S. Bravyi, M. B. Hastings, F. Verstraete, *Phys. Rev. Lett.* **97**, 050401 (2006).
30. Y. Lahini *et al.*, *Phys. Rev. A* **86**, 011603 (2012).

ACKNOWLEDGMENTS

The authors thank the Laboratory of Microfabrication, University of Science and Technology of China, Institute of Physics CAS, and National Center for Nanoscience and Technology for supporting the sample fabrication. The authors also thank QuantumCTek Co., Ltd., for supporting the fabrication and the maintenance of room-temperature electronics. **Funding:** This research was supported by the National Key Research and Development Program of China (grant nos. 2017YFA0304300, 2016YFA0302104, 2016YFA0301200, and 2017YFA0303703), the Chinese Academy of Science and its Strategic Priority Research Program (grant no. XDB28000000), Alibaba Cloud, and the Science and Technology Committee of Shanghai Municipality. This research was also supported by NSFC (grant nos. 11574380, 11774022, 11774406, 11874212, U1530401, 11890704, and U1801661), AFOSR (grant no. FA9550-14-1-0040), AOARD (grant no. FA2386-18-1-4045), ARO (grant no. W911NF-18-1-0358), JSPS, JST (Q-LEAP and CREST grant no. JPMJCR1676), and Anhui Initiative in Quantum Information Technologies. **Author contributions:** X.Z., H.F., and J.-W.P. conceived the research. Y.-R.Z., M.G., Z.Y., K.X., J.Q.Y., F.N., H.F., and X.Z. designed the experiment. Y.Z. designed the sample. H.D., Z.Y., and H.R. prepared the sample. Z.Y., M.G., Y.W., S.L., and C.W. carried out the measurements. Y.W. developed the programming platform for measurements. Y.-R.Z. performed numerical simulations. Z.Y., Y.-R.Z., and M.G. analyzed the results. F.L., J.L., Y.X., C.G., L.S., and C.-Z.P. developed room-temperature electronics equipment. All authors contributed to discussions of the results and the development of the manuscript. X.Z. and J.-W.P. supervised the whole project. **Competing interests:** None declared. **Data and materials availability:** All data needed to evaluate the conclusions in the paper are present in the paper or the supplementary materials.

SUPPLEMENTARY MATERIALS

science.sciencemag.org/content/364/6442/753/suppl/DC1
Materials and Methods
Supplementary Text
Figs. S1 to S20
Table S1
References
Movie S1

23 November 2018; accepted 17 April 2019
Published online 2 May 2019
10.1126/science.aaw1611

Downloaded from https://www.science.org at Westlake University on May 17, 2024